Electrical and Optical Enhancement Properties of Metal/Semimetal Nanostructures for Metal Oxide UV Photodetectors

36

Shayla Sawyer and Dali Shao

Introduction

UV photodetectors have been investigated for various commercial and military applications, such as secure space-to-space communications, pollution monitoring, water sterilization, flame sensing, and early missile plume detection [1]. To date, epitaxially grown or bulk wide bandgap semiconductors such as GaN, AlN, AlGaN, C (diamond), and SiC have been used for ultraviolet detection [2–12]. Fabrication of devices from these materials is often expensive with intricate processes. Also organic semiconductor materials are an attractive alternative [13, 14], though they lack the carrier mobility of inorganic semiconductors. Metal oxide semiconductor nanomaterials have the advantages of low processing cost, ease of fabrication, a large surface-to-volume ratio with carrier and photon confinement, and amenability to surface functionalization for hybrid inorganic–organic configurations. Furthermore, the unique combination of the carrier transport mechanism and oxygen adsorption/desorption processes on the nanostructures surface leads to a high internal gain. However, they also lead to slow transient response with response time on the order of seconds.

Significant enhancement of photodetector performance can be enabled by layers of metal/semimetal nanostructures. The trade-off between sensitivity and time response may be significantly reduced with careful design of metallic nanostructures relative to metal oxide active regions. The primary mechanisms for enhancement include surface plasmon resonance and carrier transfer to highly conductive materials. Details of the fundamental concepts, parameters of influence, and comparisons of enhanced devices are presented.

S. Sawyer (✉) • D. Shao
Electrical, Computer, and Systems Engineering Department, Rensselaer Polytechnic Institute, Troy, NY, USA
e-mail: sawyes@rpi.edu

B. Bhushan et al. (eds.), *Handbook of Nanomaterials Properties*,
DOI 10.1007/978-3-642-31107-9_49,

Metal Oxide UV Photodetector

Materials

Metal oxides have been developed with a range of quantum confinement options from bulk, single crystals to 0D quantum dots. Much attention has been placed on nanoscale dimensions. For ultraviolet detection, ZnO has led the way as the most prominent semiconductor among the metal oxides, though In_2O_3, SnO_2, Ga_2O_3, WO_3, and CeO_2 are all viable materials for either solar-blind or visible-blind applications. Table 36.1 shows their basic properties.

Detection Mechanism

The mechanism for ultraviolet detection and subsequent carrier transport for metal oxide nanostructures is the cause of the high photocurrent-to-dark-current ratio characteristic of these materials. A significant change of conductance upon the UV illumination can be described by the following semiquantitative model as described in Wu et al. [15] (Fig. 36.1):

$$G = G_0 \exp\left(-\frac{q\psi_s}{kT}\right)$$

The activation energy, $q\psi_s$, is located in the interspace between nanocrystals, k is the Boltzmann constant, and T is the absolute temperature. Electrons must overcome the barrier $q\psi_s$; thus, the conductance is exponentially dependent on the barrier height. In the dark, due to the affinity between the oxygen molecules and electrons, oxygen molecules adsorb onto metal oxide surface and capture nearby electrons to form negatively charged oxygen ion layer. This process can be represented by

$$O_2(g) + e^- \rightarrow O_2^-(ad)$$

As a result, a depletion layer is formed near the surface of metal oxide and the barrier height increases, which results in reduced carrier concentration and low conductance. For low-dimensional metal oxide materials, this effect can be extremely strong due to the high surface-to-volume ratio, and the depletion region created in the oxygen adsorption process can extend throughout the entire film. Upon exposure to light with photon energy above the bandgap of the metal oxide, electron–hole pairs are generated.

$$h\upsilon \rightarrow e^- + h^+$$

The photogenerated holes migrate to the surface of metal oxide and discharge the negatively charged adsorbed oxygen ions through surface electron–hole recombination.

Table 36.1 Summary of metal oxides for ultraviolet detection

Metal oxides	Crystal structure	Bandgap (eV)	Spectrum[a]
ZnO	Hexagonal	3.37	UV A
In_2O_3	Cubic/ rhombohedral	3.5–3.7	UV A (direct)
		2.9	Blue (indirect)
SnO_2	Tetragonal	3.6	UV A
Ga_2O_3	Monoclinic	4.2–4.9	UV B-UV C
WO_3	Monoclinic	3.3	UV A
CeO_2	Cubic	3.2	UV A

[a]Ultraviolet A (3.10–3.94 eV, 400–315 nm), ultraviolet B (3.94–4.43 eV, 315–280 nm), ultraviolet C (4.43–12.4 eV, 280–100 nm)

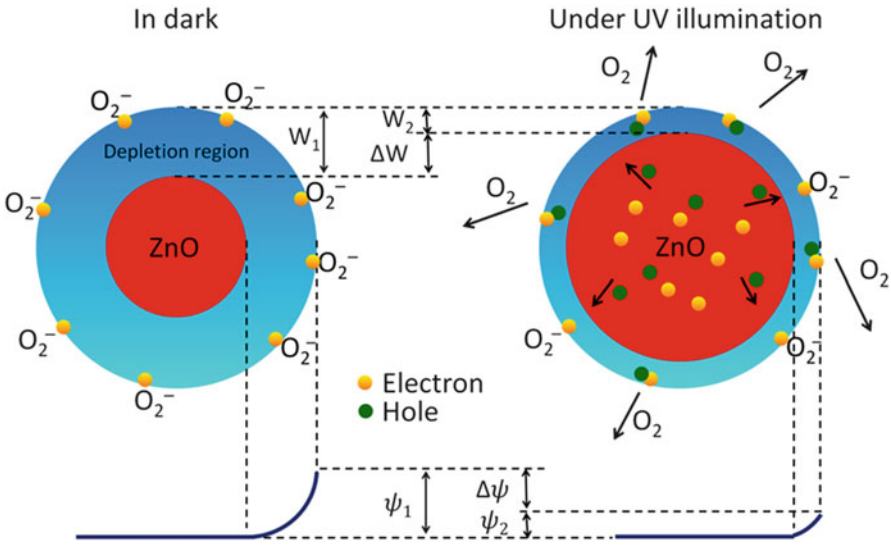

Fig. 36.1 Depletion region and potential barrier for (**a**) UV off and (**b**) UV on (Modified from [15])

$$h^+ + O_2^-(ad) \rightarrow O_2(g)$$

The barrier and depletion width decreases, and thus, the photocurrent exponentially increases until saturation.

The strong influence of surface effects on the high internal gain also results in a slow transient response. The slow decay time can be attributed to the persistent photoconductivity (PPC) phenomenon. Prades et al. discuss the origin and models for PPC in ZnO nanowires specifically through the principle that can be applied to all metal oxide nanostructures [16]. Two opposite models are proposed. The first is due to bulk defects between shallow and deep energy levels, while the second is

a pure surface effect with the capture of electrons by surface states. The relative persistence of conductance, G, is defined as $\frac{\Delta G}{G_0}$ where G_0 is the initial value in darkness. For the metal oxide nanowire, the electron–hole pairs created by UV photons give a photoresponse (ΔG_{ph}) with excess carriers (Δn, Δp):

$$\Delta G_{ph} \propto \Delta n = \Delta p = \frac{g}{1/\tau_{bulk} + 1/\tau_{surf}}$$

where g is the photogeneration rate of carriers per unit volume and τ_{bulk} and τ_{surf} are the lifetimes of photocarrier recombination in the bulk and at the surface. When surface states dominate, which is the case with nanostructures, oxygen adsorbs on the surface to separate holes from electrons forming a built-in potential. The recombination rate is significantly reduced and strongly dependent on oxygen content in air.

Photodetector Figures of Merit

Commonly used figures of merit for photodetectors are summarized in Table 36.1. Responsivity and normalized detectivity are both measures of detector sensitivity. Responsivity is essentially a measure of the effectiveness of the detector to take a given light input and convert it to current. The responsivity can be expressed by

$$R = \frac{i_{out}(\lambda, f)}{P_{in}} \quad \text{A/W}$$

where i_{out} is the photogenerated current of the detector, measured in amperes (A), and P_{in} is the incident radiation power, measured in watts (W).

Noise-equivalent power (NEP) is another basic indicator of the performance of a photodetector, which is defined as the signal power that gives a signal-to-noise ratio of one in a one hertz output bandwidth. The NEP can be expressed by the following equation:

$$NEP = \frac{i_n}{R}$$

where the i_n is the noise current in the unit of $\text{A/Hz}^{1/2}$ and the R is the responsivity in the unit of A/W.

The term normalized detectivity (D^*) is proportional to the reciprocal of the NEP and is independent of the detector area. It is therefore a popular measure of the intrinsic merit of a photodetector material:

$$D^* = \frac{\sqrt{A \times \Delta f}}{NEP} \quad \text{Jones} \left(\text{cm}\sqrt{\text{Hz}}/\text{W}\right)$$

where A is the active area in cm^{-2} and Δf is the operating bandwidth in hertz (unity: 1Hz). On the assumption that noise current is dominated by shot noise in the dark current $\left(i_n = i_{shot} = \sqrt{2qi_{dc}\Delta f}\right)$,

$$D^* = R\sqrt{\frac{A}{2qi_{dc}}} \quad \text{Jones}$$

where i_{dc} is dark current.

The dark current is measured current under dark conditions. When divided by the active area of the device, it becomes dark current density. Often a photocurrent-to-dark-current ratio is defined for a given bias.

The quantum efficiency (QE or η) is another measure of the effectiveness of the radiant energy producing electrical current in a detector. It is the ratio of photogenerated carriers and incident photons.

$$\eta = \frac{i_{out}}{q} \times \frac{hv}{P_{in}}(100)\ \%$$

The relationship between η and R is defined by the following equation:

$$R = \frac{\eta\lambda(\mu\text{m})}{1.24} \quad (\text{A/W})$$

Internal gains are defined by the ratio of photogenerated carriers to absorbed photons, while external gains are defined by the ratio of photogenerated carriers to incident photons. Overall the gain of a photodetector defines the number of electron–hole pairs produced from one photon.

The time or transient response of photodetectors is defined in both rise time and fall time. The incident light source is switched on and off at a sufficient frequency to determine the detector's ability to respond to pulsed light. Rise time is measured between 10 % and 90 % as current increases, while fall time is measured between 90 % and 10 % as current decreases.

Detector types for ultraviolet detection using metal oxides include photoconductors (PC), photodiodes (PD), metal–semiconductor–metal (MSM), metal insulator semiconductor (MIS), and field effect transistors (FET). Figure 36.2 shows schematics of device structures.

Performance Comparison

ZnO Photodetectors

ZnO materials possess various attractive characteristics for ultraviolet optoelectronic devices with reported bandgap values ranging from 3.2 to 3.4 eV, a large excitonic binding energy (60 meV), high radiation harness, amenability to wet chemical etching, and a relatively low growth temperature.

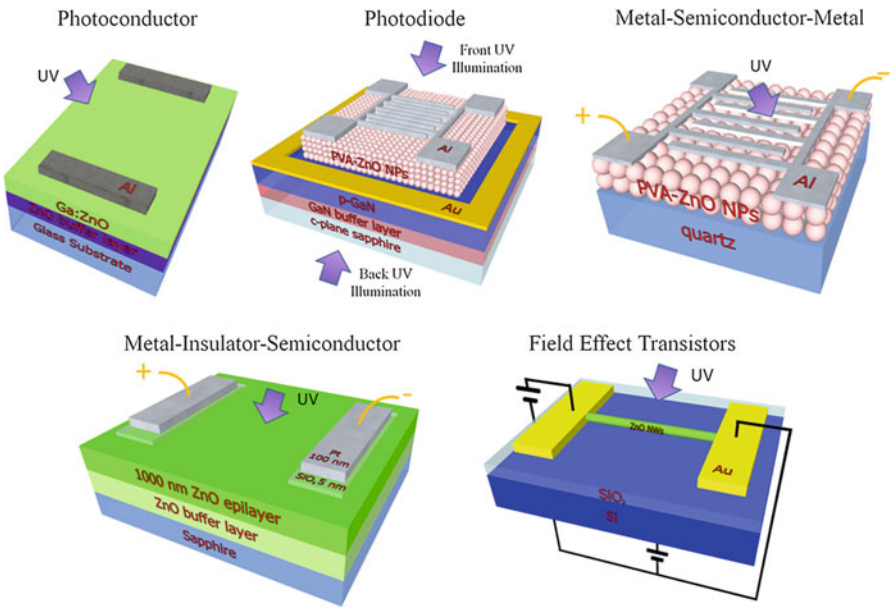

Fig. 36.2 Device design examples of ultraviolet photodetectors (Modified from [17–21])

Table 36.2 compares devices for metal oxides using selected figures of merit. Thin films have been developed by various deposition techniques including RF magnetron sputtering [22], molecular beam epitaxy (MBE), metalorganic chemical vapor deposition (MOCVD), pulsed laser deposition (PLD), and the sol–gel process. In 2000 and 2001, Liu et al. developed metal–semiconductor–metal and Schottky UV photodetectors with high-quality, epitaxially grown, ZnO thin films using MOCVD [23, 24]. Yang et al., in 2002, were the first to discover extreme sensitivity to ultraviolet light with ZnO nanowires (1D nanostructures), grown using a vapor phase transport process [25]. In 2007, Soci et al. investigated the inherent internal gain mechanism and consequential slow transient response of ZnO nanostructures [26]. Solution-processed colloidal nanoparticles (0D nanostructures) were developed by Jin et al. in 2008. The existence of persistent photoconduction found in solution-processed hybrid inorganic–organic nanostructures resulting in slower response time was investigated by Li et al. (Table 36.3).

Sawyer et al. explored surface passivation, increasing photocurrent sensitivity, for high-quality ZnO nanocrystals made by top-down wet-chemical etching technique developed by Dutta et al. [36, 38].

Other Metal Oxide UV Photodetectors

Research has expanded detection wavelengths throughout the UV range with materials such as indium oxide (In_2O_3), tin dioxide (SnO_2), gallium oxide (β-Ga_2O_3), and cerium oxide or ceria (CeO_2). Though typically the detection

Table 36.2 Photodetector figures of merit

Figure-of-Merit	Symbol/ acronym	Unit	Definition
Responsivity	R	A/W	Photocurrent divided by incident optical power
Normalized detectivity	D^*	$\text{cm}\frac{\sqrt{\text{Hz}}}{\text{W}}$ (Jones)	Measure of detector sensitivity that enables comparison even when detector area and bandwidth are different
Dark current	I_d	A	Current in the absence of light
Dark-current density	J_d	A cm^{-2}	Current divided by device active area in the absence of light
UV photogenerated current to dark current ratio	UV/dark ratio	*Unitless*	
External quantum efficiency	*EQE* or η	%	The ratio of photogenerated carriers to photon incident on the device
Internal gain	G_{int}	*Unitless*	Ratio of photogenerated carriers to photon absorbed
External gain	G_{ext}	*Unitless*	Ratio of photogenerated carriers to photon incident $G_{ext} = \eta \times G_{int}$
Noise-equivalent power	*NEP*	$\text{W}/\sqrt{\text{Hz}}$	Minimal detectable power, the optical signal in watts at which the electrical signal of noise ratio is unity when the bandwidth is limited to 1 Hz
Response time or transient response	t_r *rise time*	s	Amount of time required for current to rise from 10 % to 90 % of maximum current
	t_f *fall time*		Amount of time required for current to fall from 90 % to 10 % of maximum current

mechanisms are the same, physical properties of each material vary which contribute to differences in device performance.

Tin-doped indium oxide (ITO) is a pervasive material in electronics and photonics for its use as a transparent conducting electrode. However, the electronic and optical properties of undoped indium oxide, In_2O_3, especially in nanostructure form, have only recently been investigated. In 2001, Liang et al. were among the first to measure the semiconducting properties of In_2O_3 nanofibers grown by gold-seeded vapor–liquid–solid (VLS) mechanism [39]. Since then, nanowires, nanotowers, nanopyramids, and colloidal nanoparticles have been characterized for their electronic and optical properties [39–47]. However, the complete photoresponse including responsivity and time response of an In_2O_3 ultraviolet photodetector was only recently investigated [48]. A maximum responsivity of 11 A/W was observed at 340 nm, and the rise and fall times were 1,100 and 3,200 s, respectively.

Tin oxide (SnO_2) materials were historically researched for use as a conductive electrode and antireflective coating due to its transparency to visible light. As a wide bandgap material (3.6 eV), its potential as an ultraviolet detector has been explored with the creation of FETs and photoconductors using SnO_2 nanowire,

Table 36.3 Performance comparison of ZnO photodetectors

Ref.	Year	λ (nm)	Responsivity (A W^{-1})	Dark current (A)	Area (cm^2)	D^* (cm. $Hz^{0.5}$. W^{-1})	Time response (s)		Device type	Material
							Rise time	Fall time		
[23]	2000	300–373	400	4.50×10^{-7}	–	–	1×10^{-6}	1.5×10^{-6}	MSM	Epitaxial thin film MOCVD
[24]	2000	300–385	1.5	1×10^{-9}	1.77×10^{-4}	1.12×10^{12}	1.2×10^{-8}	5×10^{-8}	MSM	Epitaxial thin film MOCVD
[26]	2007	245–385	3.33×10^{4}	10^{-9}	3×10^{-7}	2.04×10^{13}	~50	>100	PC	Nanowires
[27]	2008	370–395	61	1.2×10^{-10}	3.14×10^{-2}	1.91×10^{15}	25	120	MSM	Colloidal nanoparticles
[22]	2007	300–384	2,069	2.22×10^{-6}	8.85×10^{-3}	2.31×10^{14}	–	–	MSM	Thin film grown by RF sputtering
[17]	2008	300–400	8.9×10^{-2}	4.11×10^{-7}	4×10^{-4}	4.91×10^{9}	–	–	MSM	Epi layer grown by RF plasma-assisted MBE (Omni Vac) on sapphire (0001) substrates
			8.3×10^{-3}	2.22×10^{-10}	4×10^{-4}	1.97×10^{10}	–	–	MIS	
[28]	2008	300–400	0.18	1.8×10^{-5} (A/cm^2)		7.5×10^{10}	–	–	–	Nanorods
[29]	2008	300–420	0.68	9.4×10^{-7} (A/cm^2)		1.24×10^{12}	<0.2	<0.2	PD	Nanoparticles
[30]	2009	325–375	12.5	–	–	–	–	–	–	Nanoparticles
[31]	2009	310–450	1×10^{-4}	4×10^{-13}	1.2×10^{-4}	3.06×10^{9}	48	0.9	PC	Nanoparticles

[32]	2009	115–400	3.3×10^{-10}	4.1×10^{-9}	4×10^{-6}	18.22	>1,000 ms	–	MSM	Lateral nanowires on a ZnO: Ga/glass template
[33]	2009	300–370	0.011	4.32×10^{-9}	0.24	1.45×10^{11}	–	–	MSM	Nanowires
[34]	2009	400–600	1.5×10^{-5}	–	–	–	–	–	PC	ZnO-infiltrating CQD films
[15]	2010		4.29×10^{-5}	2.23×10^{-9}	25	8.03×10^{9}	–	–	PC	Nanowires and nanoparticles
[35]	2010	200–425	0.02287	2×10^{-9} (A/cm^2)		9.04×10^{11}	1	–	PD	Polymer/nanoparticle bilayer
[36]	2010	200–380	0.33	4.88×10^{-12}	7.85×10^{-3}	2.34×10^{13}	100	25	PC	PVA-coated colloidal nanoparticles
[18]	2010	200–380	731.42	2.91×10^{-12}	6.24×10^{-3}	5.98×10^{16}	0.6	8	MSM	Colloidal nanoparticles
[19]	2013	320–380	1.19×10^{-4}	4.2×10^{-13}	7.85×10^{-3}	2.88×10^{10}	0.025	0.05	PD	Back-illuminated p-GaN/ZnO nanoparticle heterojunction diode
[37]	2013	365	6.83×10^{1}	6.83×10^{-9}		1.46×10^{15}	0.034	0.132	PC	Nanorods passivated by TOPO

nanobelts, and nanonets. These materials were fabricated using the vapor–liquid–solid process [49–51], laser ablation [52], and thermal evaporation [53]. A SnO_2 nanonet photoconductor was fabricated using a colloid crystal polymer template which forms a 2D ordered semiconducting nanofilm with hole sizes that can be adjusted by the mean diameter of the polymer colloidal spheres. Though responsivity characterization for ultraviolet photodetectors has not yet been reported, FET devices demonstrated on/off ratios of 10^3 and 10^5 with nanowire and nanobelts, respectively [52, 53]. High gain values have also been reported for the photoconductor devices up to 1.32×10^7 for SnO_2 nanowires [49, 50].

Solar-blind detection below 290 nm has been demonstrated with β-Ga_2O_3. Its bandgap has been reported with values between 4.2 and 4.9 eV. Photodetectors were fabricated using thermal evaporation and a single-step chemical vapor deposition process. In recent work, a bridged nanowire photoconductor demonstrated a high 250–280 nm rejection ratio of 2×10^4 and a high photocurrent-to-dark-current ratio of 3×10^4 [54]. In comparison to In_2O_3- and ZnO-based photodetectors, the bridged β-Ga_2O_3 NWs photoconductor can achieve much faster transient response with decay times less than 20 ms. The fast transient response is attributed to the extremely low electron density of β-Ga_2O_3 NWs in dark environment, which significantly suppressed the formation of surface states that originate from oxygen adsorption process [55, 56]. Therefore, the PPC phenomenon was greatly reduced in that oxygen adsorption has a nearly negligible effect on conductance.

Ceria or cesium oxide CeO_2 and tungsten oxide WO_3 are lesser-known metal oxides for UV detection. Ceria have reported bandgap values of 3.2 eV and 3.3 eV, respectively. Both were developed as nanowire devices [57–59] and possess similar high gain values and longtime responses as In_2O_3 and ZnO materials (Table 36.4).

Nanostructures for Performance Enhancement

Research to improve sensitivity and transient response of photodetectors is being pursued across the UV, visible, and infrared (IR) wavelength regions. To date, much of the research has focused on wavelengths from the visible to IR region. Until only recently investigations of enhancement for shorter UV wavelengths begun [61]. Mechanisms for performance enhancement can be categorized as either plasmonic interactions with an electric field induced by metal/semimetal nanostructures or carrier transfer from metal oxide active regions to highly conductive materials. Surface plasmon resonance (SPR) and carrier transfer concepts are described below with examples of nanostructures and performance comparisons.

Surface Plasmon Resonance Mechanisms

Metallic nanostructures absorb light due to the coherent oscillation of conduction band electrons induced by the interacting electromagnetic field. An incident

Table 36.4 Performance comparison of In_2O_3, SnO_2, β-Ga_2O_3, CeO_2, and WO_3

Ref.	Year	λ (nm)	Responsivity (A W^{-1})	UV-to-dark-current ratio	Dark current (A)	Area (cm^2)	D^* (cm. $Hz^{0.5}.W^{-1}$)	Time response (s)		Type	Material
								Rise time	Fall time		
[44]	2012	280–470	1.82	1.2×10^2	1.8×10^{-9}	7.85×10^{-3}	6.72×10^{12}	35	48	PC	In_2O_3-milled nanorods
[48]	2012	250–500	11	80	1.0×10^6	6.24×10^{-3}	1.54×10^{12}	500	1,600	MSM	In_2O_3 PVA-coated nanoparticles
[52]	2003	–	–	1×10^3	$\sim 3.8 \times 10^{-8}$	$\sim 3.8 \times 10^{-11}$	–	–	–	FET	SnO_2 nanowires
[53]	2007	–	–	1×10^5	4.0×10^{-10}	–	–	–	–	FET	SnO_2 nanobelts
[60]	2012	210–630	–	3.5	6.55×10^{-5}	–	–	>50 s	>50 s	PC	SnO_2 nanonets
[50]	2008	–	–	10^5	3.2×10^{-8}	–	–	–	–	PC	SnO_2 nanowires
[56]	2006	254	–	6.67×10^2	1.5×10^{-11}	–	–	0.22	0.09	PC	β-Ga_2O_3 nanowires
[54]	2010	254	–	3.0×10^4	2.0×10^{-13}	–	–	–	< 0.02	PC	Bridged β-Ga_2O_3 nanowires
[59]	2007	254	–	40	2.50×10^{-10}	–	–	30	300	PC	CeO_2 nanowires
[58]	2011	375	–	–	–	–	–	3	20	FET	WO_3 nanowires
[57]	2010	280–320	–	1.5×10^2	1.00×10^{-10}	–	–	100	150	PC	WO_3 nanowire

photon coupled to the electron oscillations results in an absorption band. This is known as surface plasmon resonance (SPR). Figure 36.3 demonstrates this phenomenon in detail [62]. Polarization within the metal sphere is induced by the incoming light where the separation of free electrons with respect to the ionic core results in the need for a force to restore the system. The dipolar oscillation of electrons is the surface plasmon oscillation. The size, shape, distance between nanostructures, and material all have an effect on the resonant wavelength. The electromagnetic interaction with metal gratings was first documented in 1902 by R. Wood [63]. The Mie Theory, developed in 1908, begins to create a working model for the optical properties that result with isolated metal nanoparticles. Specifically, it is a mathematical description of the scattering of electromagnetic reaction by spherical particles in a continuous medium [64]. Fano et al. first described plasmons from incident electromagnetic radiation on metallic gratings as "superficial waves traveling with momentum along the surface of the grating and exponentially damped in the normal direction" [65]. In the review article by Ghosh et al., the assumptions, application, and limitations of the Mie Theory for plasmonic systems are thoroughly analyzed [64]. For isolated nanoparticles less than 100 nm in diameter, the Mie Theory can be reduced to the following relationship:

$$\sigma_{ext} = 9\frac{\omega}{c}\epsilon_m^{3/2}V\frac{\epsilon_2(\omega)}{[\epsilon_1(\omega)+2\epsilon_m]^2+[\epsilon_2(\omega)]^2}$$

where $V = (4\pi/3)R^3$ is the volume of the spherical particle, ω is the angular frequency of the exciting light, c is the velocity of light, and ϵ_m and $\epsilon_1(\omega) + i\epsilon_2(\omega)$ are the dielectric functions of the surrounding medium and the material itself, respectively. The resonance condition is fulfilled when $\epsilon_1(\omega) = -2\epsilon_m$ if ϵ_2 is small or weakly dependent on ω. Nanoparticles larger than 100 nm require a correction factor that results in the broadening and red-shifting of the resonance frequency. Non-spherical nanoparticles also require a correction factor to more accurately predict the resonant frequency.

There is an ongoing debate about the exact mechanism responsible for enhancement in grating structures. Crouse and Keshavareddy weighed the significance of electromagnetic modes responsible for transmittance peaks including horizontally oriented surface plasmons (HSPs), Wood-Rayleigh (WR) anomalies, vertical surface resonances (VSRs), diffracted modes, and cavity modes (also called waveguide modes) [66]. Most agree that HSPs should be minimized as it has a converse affect on enhancement.

Ebbessen et al. were the first to discover enhanced optical transmission from sub-wavelength hole arrays [67]. This work spawned studies of 1D and 2D nanoarrays with slits, gratings, resonant cavities, and holes for the performance improvement of photodetectors [66, 68–76]. Collin et al. investigated the strong confinement of light by a resonant cavity on an MSM photodetector using

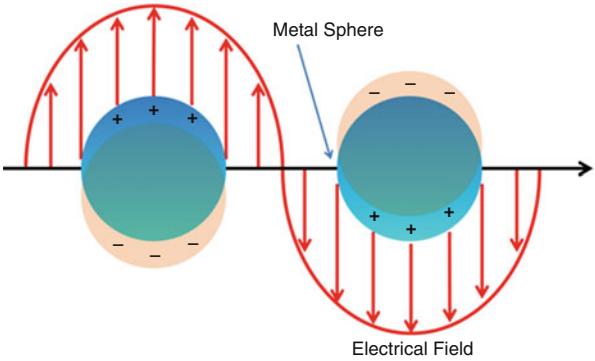

Fig. 36.3 Surface plasmon resonance (SPR) of spherical nanometal particle. A dipole oscillates in phase with the electric field of the incoming light (Modified from [62])

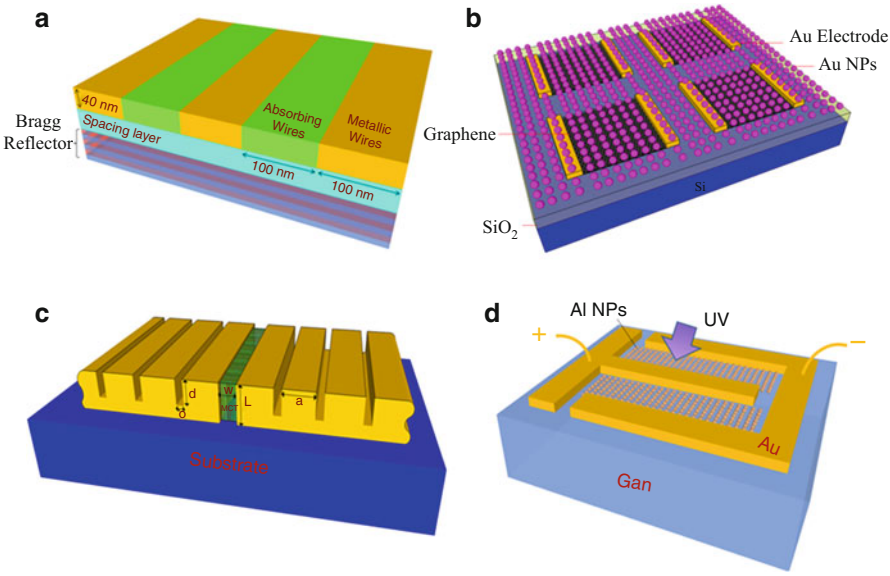

Fig. 36.4 Examples of metal nanostructures to induce surface plasmon resonance. (**a**) Alternating metal–semiconductor gratings on a Bragg reflector (Modified from [74]). (**b**) Graphene photodetector enhanced by gold nanoparticle arrays (Modified from [77]). (**c**) Nanoslit metal grating (Modified from [79]). (**d**) Aluminum nanoparticles on GaN photodetector (Modified from [78])

alternating metal–semiconductor gratings on a multilayer Bragg reflector [74]. A graphene photodetector was enhanced by gold nanoparticle arrays [77]. Plasmonic enhancement in the UV range was achieved by Butan et al. using aluminum nanoparticles deposited on a GaN MSM photodetector [78]. Schematic designs of the enhancement structures are shown in Fig. 36.4. Table 36.5 is a cross section of the experimental research results for plasmonic enhancement for various photodetectors.

Table 36.5 Surface plasmon-enhanced photodetectors across UV–vis-IR spectrum

Ref.	Year	Plasmonic structure	Material (semiconductor/metal plasmonic)	Device structure	λ (nm)	Enhancement factor
[76]	1998	Island nanoparticles	Si/Au	SOI-MSM	Near-IR (800 nm)	18× photocurrent enhancement
[80]	2002	Metallic gratings	Ge/Au	MSM	IR	8× absorption enhancement factor
[74]	2004	Metal–semiconductor grating	GaAs/alternating Ag and GaAs	MSM	IR	9× enhancement of external quantum efficiency
[77]	2011	Nanoparticle array	Graphene/Au	MGM*	Green-Red (530–633 nm)	Order of magnitude improvement in QE >800 % increase in photocurrent
[81]	2006	Nanoslit(s)	HgCdTe/Au	–	Mid-IR (10 μm)	1 slit 10× enhancement factor 20 periods 250× enhancement factor
[82]	2005	Nanoparticles	Si/Au	PN junction diode	Red (640 nm)	50–80 % increase in photocurrent
[78]	2012	Nanoparticle array	GaN/Al	MSM	UV (340 nm)	50 % enhancement in QE

*Average photocurrent enhancement

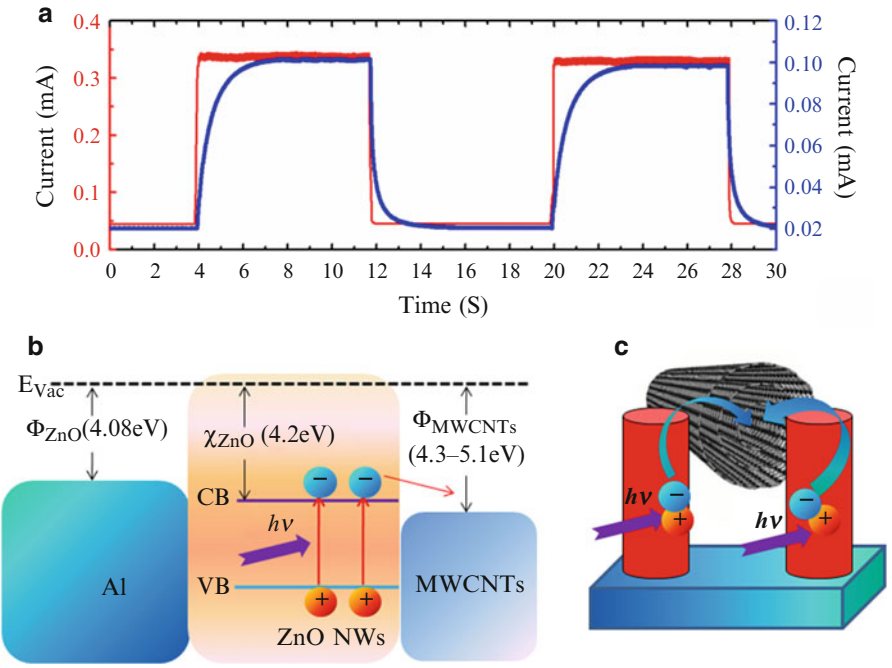

Fig. 36.5 Transient response of photodetector with MWCNT (*red*) and without MWCNT (*blue*) (**b**) Energy band diagram of Al/ZnO NWs/MWCNT system. (**c**) Carrier transport process of ZnO NWs/MWCNT interface (Republished with permission from [98])

Carrier Transfer Mechanisms

It is well known that the photoresponse of metal oxide materials is sensitive to film thickness, deposition temperature, annealing treatments, and doping. It has been shown that aspects of device performance can therefore be improved by optimizing these parameters [83–88]. Further enhancement with the addition of metal/semi-metal layers is an approach to circumvent issues inherent to most metal oxides attributed to the slow chemisorption of oxygen molecules [16].

In 2007, Yadav et al. were the first to study the interfacial charge-transfer kinetics between ultrathin layers of different metals with a metal oxide thin film [89]. In this work, enhanced photoresponse was due to the effective transfer of electrons from the metal to ZnO at the interface, and the injected charge carriers compensate the surface states and increase the photoconductivity. The UV/dark current ratio improved by more than 5× with Te/ZnO bilayer. Nevertheless, the rise and fall times significantly increased, demonstrating the common trade-off in photodetectors. Tzeng et al. continued the concept of interfacial charge transfer by modifying the interface using Ag nanoparticles. The photocurrent-to-dark-current contrast ratio increased by almost 74 times. The decay time was reduced from 824 to 36 s, and the rise time was also reduced from ~151 to 4 s after depositing Ag NPs [90]. These results are

Table 36.6 Carrier transfer enhancement of UV photodetectors

Ref.	Year	Carrier transfer enhancement material	Semiconductor material	Device structure	λ (nm)	Enhancement factor
[92]	2010	Embedded graphene layer	ZnO QD-polymer		365 nm	~330× photocurrent
[89]	2007	Metal thin sheet: Te, Au, Pb, Cu, Sn, Al	ZnO thin film	Bilayer	365 nm	5× UV/dark current ratio (Te)
[90]	2012	Ag NP	ZnO NW		365 nm	74× UV/dark current ratio
						37× faster rise time
						23× faster fall time
[101]	2013	Graphene core-shell	ZnO NP	PC	335 nm	3 orders of magnitude rise and fall time improvement
[98]	2013	MWCNT	ZnO NW/p-Si	PD	335 nm	3× improvement responsivity
						23× faster rise time
						18× faster fall time
[94]	2013	Graphene core–shell	WO_3	MSM	340 nm	100× faster time response
[99]	2012	Graphene QD	ZnO NP	MSM	335 nm	2× improvement responsivity
						50× faster rise time
						37× faster fall time

attributed to the formation of AgO_x at the interface between Ag and ZnO, which increased the Schottky barrier height and led to a significant enhancement in the charge-transfer kinetics near the interface of ZnO and AgO_x.

Carbon nanomaterials, specifically carbon nanotubes (CNTs) and graphene, have been investigated in hybrid nanocomposites to provide improved charge separation and subsequent carrier transport [91–97]. CNT hybrid materials have proven to be a versatile electrode for fuel-cell, photodetector, and supercapacitor applications for their solution processable fabrication, high conductivity, mechanical flexibility and strength, and dimension variability. Recently, Shao et al. demonstrated a multiwalled carbon nanotube (MWCNT)/ZnO NW/p-Si photodiode with rise and fall times of 0.09 s and 0.08 s, respectively. This is at least 20 times faster than ZnO NW/p-Si photodiode without using MWCNTs. In addition to improved transient response, the maximum responsivity of the photodiode employing MWCNTs enhanced by three times, which can reach to 4.7 A/W for UV light (365 nm) at 2 V bias [98]. The improved performance is explained by the band diagram in Fig. 36.5. Electrons transfer from ZnO to MWCNTs because it is energetically favorable to do so. Due to the semimetallic property of the MWCNTs, the composite structure has much better conductivity than the bare ZnO NWs array. This effectively improved the carrier transport and collection efficiency.

Graphene has many unique properties including high carrier transport mobility, superior mechanical properties, excellent chemical stability, larger surface area than CNTs, and low cost. Thin graphene sheet layers, quantum dots, and core-shells are common structures for nanocomposites with metal oxides for improved carrier transport [93, 94, 97, 99]. Graphene-CdS quantum dot nanocomposites were explored through facile fabrication processes by Wu et al. and Cao et al. as methods to enhance conductivity of quantum dot layers. Williams et al. were among the first to create graphene metal oxide nanocomposites for conductivity improvement [100]. Recently, graphene quantum dots, synthesized by the hydrothermal method, were used to enhance the performance of ZnO-based ultraviolet photodetectors through the preferential carrier transfer to the more conductive material [99]. The rise and fall times reduced from longer than 3 s each to 0.06 s and 0.08 s, respectively, while a high responsivity of >450 A/W at 375 nm was maintained [99]. Similar results were obtained with a ZnO NPs-graphene core-shell structure [94, 101] (Table 36.6).

Summary

Metal oxides and their nanostructures have many advantages for ultraviolet detection including low cost, a high surface-to-volume ratio, and a large internal gain mechanism. A long transient response due to the adsorption of oxygen on the semiconductor surface limits performance. Metal and semimetal nanostructures can improve overall performance by inducing surface plasmon resonance or allowing the transfer of carriers to more conductive material.

References

1. Blank TV, Gol'dberg YA (2003) Semiconductor photoelectric converters for the ultraviolet region of the spectrum. Semiconductors 37:999–1030
2. Zhang SK, Wang WB, Shtau I, Yun F, He L, Morkoc H, Zhou X, Tamargo M, Alfano RR (2002) Back-illuminated GaN/AlGaN heterojunction ultraviolet photodetector with high internal gain. Appl Phys Lett 81(25):4862–4864. doi:10.1063/1.1526166
3. Xu GY, Salvador A, Kim W, Fan Z, Lu C, Tang H, Morkoc H, Smith G, Estes M, Goldenberg B, Yang W, Krishnankutty S (1997) High speed, low noise ultraviolet photodetectors based on GaN p-i-n and AlGaN(p)-GaN(i)-GaN(n)structures. Appl Phys Lett 71(15):2154–2156
4. Chen X, Zhu H, Cai J, Wu Z (2007) High-performance 4H-SiC-based ultraviolet p-i-n photodetector. J Appl Phys 102(2):024505. doi:10.1063/1.2747213
5. Whitfield MD, Chan SSM, Jackman RB (1996) Thin film diamond photodiode for ultraviolet light detection. Appl Phys Lett 68(3):290–292. doi:10.1063/1.116062
6. Walker D, Monroy E, Kung P, Wu J, Hamilton M, Sanchez FJ, Diaz J, Razeghi M (1999) High-speed, low-noise metal–semiconductor–metal ultraviolet photodetectors based on GaN. Appl Phys Lett 74(5):762. doi:10.1063/1.123303
7. Osinsky A, Gangopadhyay S, Gaska R, Williams B, Khan MA, Kuksenkov D, Temkin H (1997) Low noise p-π-n GaN ultraviolet photodetectors. Appl Phys Lett 71(16):2334. doi:10.1063/1.120023

8. Monroy E, Omnès F, Calle F (2003) Wide-bandgap semiconductor ultraviolet photodetectors. Semicond Sci Technol 18(4):R33–R51
9. Liao M, Koide Y, Alvarez J (2005) Thermally stable visible-blind diamond photodiode using tungsten carbide Schottky contact. Appl Phys Lett 87(2):022105-022105-022103. doi:10.1063/1.1992660
10. Li J, Fan ZY, Dahal R, Nakarmi ML, Lin JY, Jiang HX (2006) 200 nm deep ultraviolet photodetectors based on AlN. Appl Phys Lett 89(21):213510–213513
11. Chen X, Yang W, Wu Z (2006) Visible blind p–i–n ultraviolet photodetector fabricated on 4H-SiC. Microelectron Eng 83(1):104–106. doi:http://dx.doi.org/10.1016/j.mee.2005.10.034
12. Chen Q, Khan MA, Sun CJ, Yang JW (1995) Visible-blind ultraviolet photodetectors based on GaN p-n junctions. Electron Lett 31(20):1781–1782. doi:10.1049/el:19951190
13. Cárdenas JR, de Vasconcelos EA, de Azevedo WM, da Silva EF, Pepe I, da Silva AF, Ribeiro SS, Silva KA (2008) A conducting polymer–silicon heterojunction as a new ultraviolet photodetector. Appl Surf Sci 255(3):688–690. doi:http://dx.doi.org/10.1016/j.apsusc.2008.07.038
14. Yu G, Pakbaz K, Heeger AJ (1994) Semiconducting polymer diodes: large size, low cost photodetectors with excellent visible–ultraviolet sensitivity. Appl Phys Lett 64(25):3422. doi:10.1063/1.111260
15. Wu JM, Chen YR, Lin YH (2011) Rapidly synthesized ZnO nanowires by ultraviolet decomposition process in ambient air for flexible photodetector. Nanoscale 3(3):1053–1058. doi:10.1039/c0nr00595a
16. Prades JD, Hernandez-Ramirez F, Jimenez-Diaz R, Manzanares M, Andreu T, Cirera A, Romano-Rodriguez A, Morante JR (2008) The effects of electron–hole separation on the photoconductivity of individual metal oxide nanowires. Nanotechnology 19(46):465501. doi:10.1088/0957-4484/19/46/465501
17. Young SJ, Ji LW, Chang SJ, Liang SH, Lam KT, Fang TH, Chen KJ, Du XL, Xue QK (2008) ZnO-based MIS photodetectors. Sens Act A: Phys 141(1):225–229. doi:10.1016/j.sna.2007.06.003
18. Qin L, Shing C, Sawyer S (2011) Metal–Semiconductor–Metal ultraviolet photodetectors based on zinc-oxide colloidal nanoparticles. IEEE Electron Device Lett 32(1):51–53
19. Qin L, Shao D, Shing C, Sawyer S (2013) Wavelength selective p-GaN/ZnO colloidal nanoparticle heterojunction photodiode. Appl Phys Lett 102(7):071106. doi:10.1063/1.4793210
20. Campos LC, Guimarães MHD, Goncalves AMB, de Oliveira S, Lacerda RG (2013) ZnO UV photodetector with controllable quality factor and photosensitivity. AIP Advances 3(2):022104. doi:10.1063/1.4790633
21. Shinde SS, Rajpure KY (2011) High-performance UV detector based on Ga-doped zinc oxide thin films. Appl Surf Sci 257(22):9595–9599. doi:10.1016/j.apsusc.2011.06.073
22. Bi Z, Zhang J, Bian X, Wang D, Zhang X, Zhang W, Hou X (2008) A high-performance ultraviolet photoconductive detector based on a ZnO film grown by RF sputtering. J Electron Mater 37(5):760–763
23. Liu Y, Gorla CR, Liang S, Emanetoglu N, Lu Y, Shen H, Wraback M (2000) Ultraviolet photodetectors based on epitaxial ZnO films grown by MOCVD. J Electron Mater 29(1):69–74
24. Liang S, Sheng H, Liu YG, Huo Z, Lu Y, Shen H (2001) ZnO schottky ultraviolet photodetectors. J Cryst Growth 22:110–113
25. Kind H, Yun H, Messer B, Law M, Yang P (2002) Nanowire ultraviolet photodetectors and optical switches. Adv Mater 14(2):158–160
26. Soci C, Zhang A, Xiang B, Dayeh SA, Aplin DPR, Park J, Bao XY, Lo YH, Wang D (2007) ZnO nanowire UV photodetectors with high internal gain. Nano Lett 7(4):1003–1009
27. Jin Y, Wang J, Sun B, Blakesley JC, Greenham NC (2008) Solution-processed ultraviolet photodetectors based on colloidal ZnO nanoparticles. Nano Lett 8(6):1649–1653

28. Lin Y-Y, Chen C-W, Yen W-C, Su W-F, Ku C-H, Wu J-J (2008) Near-ultraviolet photodetector based on hybrid polymer/zinc oxide nanorods by low-temperature solution processes. Appl Phys Lett 92(23):233301. doi:10.1063/1.2940594
29. Li H-G, Wu G, Shi M-M, Yang L-G, Chen H-Z, Wang M (2008) ZnO/poly (9,9-dihexylfluorene) based inorganic/organic hybrid ultraviolet photodetector. Appl Phys Lett 93(15):153309. doi:10.1063/1.3003881
30. Venkataprasad Bhat S, Vivekchand SRC, Govindaraj A, Rao CNR (2009) Photoluminescence and photoconducting properties of ZnO nanoparticles. Solid State Commun 149(13–14):510–514. doi:10.1016/j.ssc.2009.01.014
31. Jun JH, Seong H, Cho K, Moon B-M, Kim S (2009) Ultraviolet photodetectors based on ZnO nanoparticles. Ceram Int 35(7):2797–2801. doi:10.1016/j.ceramint.2009.03.032
32. Lu C-Y, Chang S-P, Chang S-J, Hsueh T-J, Hsu C-L, Chiou Y-Z, Chen IC (2009) A lateral ZnO nanowire UV photodetector prepared on a ZnO: Ga/glass template. Semicond Sci Technol 24(7):075005. doi:10.1088/0268-1242/24/7/075005
33. Chen KJ, Hung FY, Chang SJ, Young SJ (2009) Optoelectronic characteristics of UV photodetector based on ZnO nanowire thin films. J Alloys Compd 479(1–2):674–677. doi:10.1016/j.jallcom.2009.01.026
34. Pourret A, Guyot-Sionnest P, Elam JW (2009) Atomic layer deposition of ZnO in quantum dot thin films. Adv Mater 21(2):232–235. doi:10.1002/adma.200801313
35. Li H, Fan C, Wu G, Chen H, Wang M (2010) Solution-processed hybrid bilayer photodetectors with rapid response to ultraviolet radiation. J Phys D Appl Phys 43(42):425101. doi:10.1088/0022-3727/43/42/425101
36. Qin L, Shing C, Sawyer S, Dutta PS (2011) Enhanced ultraviolet sensitivity of zinc oxide nanoparticle photoconductors by surface passivation. Opt Mater 33(3):359–362. doi:10.1016/j.optmat.2010.09.020
37. Rostami A, Dolatyari M, Amini E, Rasooli H, Baghban H, Miri S (2013) Sensitive, fast, solution-processed ultraviolet detectors based on passivated zinc oxide nanorods. Chemphyschem: A Eur J Chem Phys Phys Chem 14(3):554–559. doi:10.1002/cphc.201200660
38. Sharma S, Tran A, Nalamasu O, Dutta PS (2006) Spin-coated ZnO thin films using ZnO nano-colloid. J Electron Mater 35(6):1237–1240
39. Liang C, Meng G, Lei Y, Phillipp F, Zhang L (2001) Catalytic growth of semiconducting In2O3 nanofibers. Adv Mater 13(17):1330–1333
40. Gali P, Kuo F-L, Shepherd N, Philipose U (2012) Role of oxygen vacancies in visible emission and transport properties of indium oxide nanowires. Semicond Sci Technol 27(1):015015. doi:10.1088/0268-1242/27/1/015015
41. Guha P, Kar S, Chaudhuri S (2004) Direct synthesis of single crystalline In[sub 2]O[sub 3] nanopyramids and nanocolumns and their photoluminescence properties. Appl Phys Lett 85(17):3851. doi:10.1063/1.1808886
42. Jean S-T, Her Y-C (2010) Growth mechanism and photoluminescence properties of In2O3 nanotowers. Cryst Growth Des 10(5):2104–2110. doi:10.1021/cg9011839
43. Li C, Zhang D, Han S, Liu X, Tang T, Zhou C (2003) Diameter-controlled growth of single-crystalline In2O3 nanowires and their electronic properties. Adv Mater 15(2):143–146
44. Qin L, Dutta PS, Sawyer S (2012) Photoresponse of indium oxide particulate-based thin films fabricated using milled nanorods grown by the self-catalytic vapor–liquid–solid process. Semicond Sci Technol 27(4):045005. doi:10.1088/0268-1242/27/4/045005
45. Shao D, Qin L, Sawyer S (2013) Optical properties of polyvinyl alcohol (PVA) coated In2O3 nanoparticles. Opt Mater 35(3):563–566. doi:10.1016/j.optmat.2012.10.026
46. Zhang D, Li C, Han S, Liu X, Tang T, Jin W, Zhou C (2003) Electronic transport studies of single-crystalline In[sub 2]O[sub 3] nanowires. Appl Phys Lett 82(1):112. doi:10.1063/1.1534938

47. Zhang D, Li C, Han S, Liu X, Tang T, Jin W, Zhou C (2003) Ultraviolet photodetection properties of indium oxide nanowires. Appl Phys A: Mater Sci Process 77(1):163–166. doi:10.1007/s00339-003-2099-3
48. Shao D, Qin L, Sawyer S (2012) Near ultraviolet photodetector fabricated from polyvinyl-alcohol coated In2O3 nanoparticles. Appl Surf Sci 261:123–127. doi:10.1016/j.apsusc.2012.07.111
49. Hu L, Yan J, Liao M, Wu L, Fang X (2011) Ultrahigh external quantum efficiency from thin SnO2 nanowire ultraviolet photodetectors. Small 7(8):1012–1017. doi:10.1002/smll.201002379
50. Lin C-H, Chen R-S, Chen T-T, Chen H-Y, Chen Y-F, Chen K-H, Chen L-C (2008) High photocurrent gain in SnO[sub 2] nanowires. Appl Phys Lett 93(11):112115. doi:10.1063/1.2987422
51. Mathur S, Barth S, Shen H, Pyun JC, Werner U (2005) Size-dependent photoconductance in SnO2 nanowires. Small 1(7):713–717. doi:10.1002/smll.200400168
52. Liu Z, Zhang D, Song H, Li C, Tang T, Jin W, Liu X, Lei B, Zhou C (2003) Laser ablation synthesis and electron transport studies of tin oxide nanowires. Adv Mater 15(20):1754–1757
53. Chen Y, Zhu C, Cao M, Wang T (2007) Photoresponse of SnO2 nanobelts grown in situ on interdigital electrodes. Nanotechnology 18(28):285502. doi:10.1088/0957-4484/18/28/285502
54. Li Y, Tokizono T, Liao M, Zhong M, Koide Y, Yamada I, Delaunay J-J (2010) Efficient assembly of bridged β-Ga2O3 nanowires for solar-blind photodetection. Adv Funct Mater 20(22):3972–3978. doi:10.1002/adfm.201001140
55. Feng P, Xue XY, Liu YG, Wan Q, Wang TH (2006) Achieving fast oxygen response in individual β-Ga[sub 2]O[sub 3] nanowires by ultraviolet illumination. Appl Phys Lett 89(11):112114. doi:10.1063/1.2349278
56. Feng P, Zhang JY, Li QH, Wang TH (2006) Individual β-Ga[sub 2]O[sub 3] nanowires as solar-blind photodetectors. Appl Phys Lett 88(15):153107. doi:10.1063/1.2193463
57. Huang K, Zhang Q, Yang F, He D (2010) Ultraviolet photoconductance of a single hexagonal WO3 nanowire. Nano Res 3(4):281–287. doi:10.1007/s12274-010-1031-3
58. Li L, Zhang Y, Fang X, Zhai T, Liao M, Sun X, Koide Y, Bando Y, Golberg D (2011) WO3 nanowires on carbon papers: electronic transport, improved ultraviolet-light photodetectors and excellent field emitters. J Mater Chem 21(18):6525. doi:10.1039/c0jm04557h
59. Fu XQ, Wang C, Feng P, Wang TH (2007) Anomalous photoconductivity of CeO[sub 2] nanowires in air. Appl Phys Lett 91(7):073104. doi:10.1063/1.2771090
60. Chen H, Hu L, Fang X, Wu L (2012) General fabrication of monolayer SnO2 nanonets for high-performance ultraviolet photodetectors. Adv Funct Mater 22(6):1229–1235. doi:10.1002/adfm.201102506
61. Qiaoqiang G, Liangcheng Z, Dierolf V, Bartoli FJ (2009) UV plasmonic structures: direct observations of UV extraordinary optical transmission and localized field enhancement through nanoslits. IEEE Photonics J 1(4):245–253. doi:10.1109/jphot.2009.2035998
62. Liang A, Liu Q, Wen G, Jiang Z (2012) The surface-plasmon-resonance effect of nanogold/silver and its analytical applications. TrAC Trends Anal Chem 37:32–47. doi:10.1016/j.trac.2012.03.015
63. Wood RW (1902) On a remarkable case of uneven distribution of light in a diffraction grating spectrum. Philos Mag 4(21):396–402
64. Ghosh SK, Pal T (2007) Interparticle coupling effect on the surface plasmon resonance of gold nanoparticles: form theory to applications. Chem Rev 107:4797–4862
65. Fano U (1941) The theory of anomalous diffraction gratings and of quasi-stationary waves on metallic surfaces (Sommerfeld's waves). J Opt Soc Am 31:213–222
66. Crouse D, Keshavareddy P (2005) Role of optical and surface plasmon modes in enhanced transmission and applications. Opt Express 13(20):7760–7771

67. Ebbesen TW, Lezec HJ, Ghaemi HF, Thio T, Wolff PA (1998) Extraordinary optical transmission through sub-wavelength hole arrays. Nature 391:667–669
68. Crouse D (2005) Numerical modeling and electromagnetic resonant modes in complex grating structures and optoelectronic device applications. IEEE Trans Electron Devices 52(11):2365–2373
69. Treacy M (2002) Dynamical diffraction explanation of the anomalous transmission of light through metallic gratings. Phys Rev B 66(19):195105. doi:10.1103/PhysRevB.66.195105
70. Collin S, Pardo F, Tessier R, Pelouard J-L (2002) Horizontal and vertical surface resonances in transmission metallic gratings. J Opt A: Appl Opt 4:5154–5160
71. Barbara A, Quémerais P, Bustarret E, Lopez-Rios T (2002) Optical transmission through subwavelength metallic gratings. Phys Rev B 66(16):161403. doi:10.1103/PhysRevB.66.161403
72. García-Vidal F, Martín-Moreno L (2002) Transmission and focusing of light in one-dimensional periodically nanostructured metals. Phys Rev B 66(15):155412. doi:10.1103/PhysRevB.66.155412
73. Cao Q, Lalanne P (2002) Negative role of surface plasmons in the transmission of metallic gratings with very narrow slits. Phys Rev Lett 88(5):057403. doi:10.1103/PhysRevLett.88.057403
74. Collin S, Pardo F, Teissier R, Pelouard J-L (2004) Efficient light absorption in metal–semiconductor–metal nanostructures. Appl Phys Lett 85(2):194. doi:10.1063/1.1771467
75. Collin SP, Pardo F, Pelouard J-L (2003) Resonant-cavity-enhanced subwavelength metal–semiconductor–metal photodetector. Appl Phys Lett 83(8):1521. doi:10.1063/1.1604942
76. Stuart HR, Hall DG (1998) Island size effects in nanoparticle-enhanced photodetectors. Appl Phys Lett 73(26):3815. doi:10.1063/1.122903
77. Liu Y, Cheng R, Liao L, Zhou H, Bai J, Liu G, Liu L, Huang Y, Duan X (2011) Plasmon resonance enhanced multicolour photodetection by graphene. Nat Commun 2:579. doi:10.1038/ncomms1589
78. Butun S, Cinel NA, Ozbay E (2012) LSPR enhanced MSM UV photodetectors. Nanotechnology 23(44):444010. doi:10.1088/0957-4484/23/44/444010
79. Porto JA, Garcia-Vidal FJ, Pendry JB (1999) Transmission resonances on metallic gratings with very narrow slits. Phys Rev Lett 83(14):2845–2848
80. Burc S, Tidin O, Okyay K (2012) Plasmonic nanoslit array enhanced metal–semiconductor–metal optical detectors. IEEE Photon Technol Lett 324(7):548–550
81. Yu Z, Veronis G, Fan S, Brongersma ML (2006) Design of midinfrared photodetectors enhanced by surface plasmons on grating structures. Appl Phys Lett 89(15):151116. doi:10.1063/1.2360896
82. Schaadt DM, Feng B, Yu ET (2005) Enhanced semiconductor optical absorption via surface plasmon excitation in metal nanoparticles. Appl Phys Lett 86(6):063106. doi:10.1063/1.1855423
83. Zhang DH (1995) Fast photoresponse and the related change of crystallite barriers for ZnO films deposited by RF sputtering. J Phys D Appl Phys 28:1273–1277
84. Studenikin SA, Golego N, Cocivera M (2000) Carrier mobility and density contributions to photoconductivity transients in polycrystalline ZnO films. J Appl Phys 87(5):2413. doi:10.1063/1.372194
85. Bikowski A, Ellmer K (2013) Electrical transport in hydrogen-aluminium Co-doped ZnO and Zn1 − xMgxO films: relation to film structure and composition. J Appl Phys 113(5):053710. doi:10.1063/1.4790314
86. Li Y, Huang Q, Bi X (2013) The change of electrical transport characterizations in Ga doped ZnO films with various thicknesses. J Appl Phys 113(5):053702. doi:10.1063/1.4789985
87. Lee JY, Choi YS, Kim JH, Park MO, Im S (2002) Optimizing n-ZnO/p-Si heterojunctions for photodiode applications. Thin Solid Films 403–404:553–557

88. Shao D, Yu M, Lian J, Sawyer S (2012) Heterojunction photodiode fabricated from hydrogen treated ZnO nanowires grown on p-silicon substrate. Appl Phys Lett 101(21):211103. doi:10.1063/1.4767679
89. Yadav HK, Sreenivas K, Gupta V (2007) Enhanced response from metal/ZnO bilayer ultraviolet photodetector. Appl Phys Lett 90(17):172113. doi:10.1063/1.2733628
90. Tzeng S-K, Hon M-H, Leu I-C (2012) Improving the performance of a Zinc Oxide nanowire ultraviolet photodetector by adding silver nanoparticles. J Electrochem Soc 159(4):H440. doi:10.1149/2.088204jes
91. Yang M-H, Liang T, Peng Y-C, Chen Q (2007) Synthesis and characterization of a nanocomplex of ZnO nanoparticles attached to carbon nanotubes. Acta Phys-Chim Sin 23(2):145–151
92. Yang HY, Son DI, Kim TW, Lee JM, Park WI (2010) Enhancement of the photocurrent in ultraviolet photodetectors fabricated utilizing hybrid polymer-ZnO quantum dot nanocomposites due to an embedded graphene layer. Org Electron 11(7):1313–1317. doi:10.1016/j.orgel.2010.04.009
93. Wu J, Bai S, Shen X, Jiang L (2010) Preparation and characterization of graphene/CdS nanocomposites. Appl Surf Sci 257(3):747–751. doi:10.1016/j.apsusc.2010.07.058
94. Shao D, Yu M, Lian J, Sawyer S (2013) Ultraviolet photodetector fabrication from WO3 nano-disks/graphene nanocomposite material. Nanotechnology 24:295701. doi:10.1088/0957-4484/24/29/295701
95. Robel I, Bunker BA, Kamat PV (2005) Single-walled carbon nanotube-CdS nanocomposites as light-harvesting assemblies: photoinduced charge-transfer interactions. Adv Mater 17(20):2458–2463. doi:10.1002/adma.200500418
96. Hou Y, Cheng Y, Hobson T, Liu J (2010) Design and synthesis of hierarchical MnO2 nanospheres/carbon nanotubes/conducting polymer ternary composite for high performance electrochemical electrodes. Nano Lett 10(7):2727–2733. doi:10.1021/nl101723g
97. Cao A, Liu Z, Chu S, Wu M, Ye Z, Cai Z, Chang Y, Wang S, Gong Q, Liu Y (2010) A facile one-step method to produce graphene-CdS quantum dot nanocomposites as promising optoelectronic materials. Adv Mater 22(1):103–106. doi:10.1002/adma.200901920
98. Shao D, Yu M, Lian J, Sawyer S (2013) Heterojunction photodiode fabricated from multiwalled carbon nanotube/ZnO nanowire/p-silicon composite structure. Appl Phys Lett 102(2):021107. doi:10.1063/1.4776691
99. Dali S, Sawyer S, Tao H, Mingpeng Y, Jie L (2012) Photoconductive enhancement effects of graphene quantum dots on ZnO nanoparticle photodetectors. In: Lester Eastman conference on high performance devices (LEC), Brown University, Providence RI, 7–9 Aug 2012, pp 1–4. doi:10.1109/lec.2012.6410972
100. Williams G, Seger B, Kamat PV (2008) TiO2-graphene nanocomposites UV-assisted photocatalytic reduction of graphene oxide. ACS Nano 2(7):1487–1491
101. Shao D, Yu M, Sun T, Lian J, Sawyer S (2013) High responsivity, fast ultraviolet photodetector fabricated from ZnO nanoparticle-graphene core/shell structure. Nanoscale 5:3664–3667